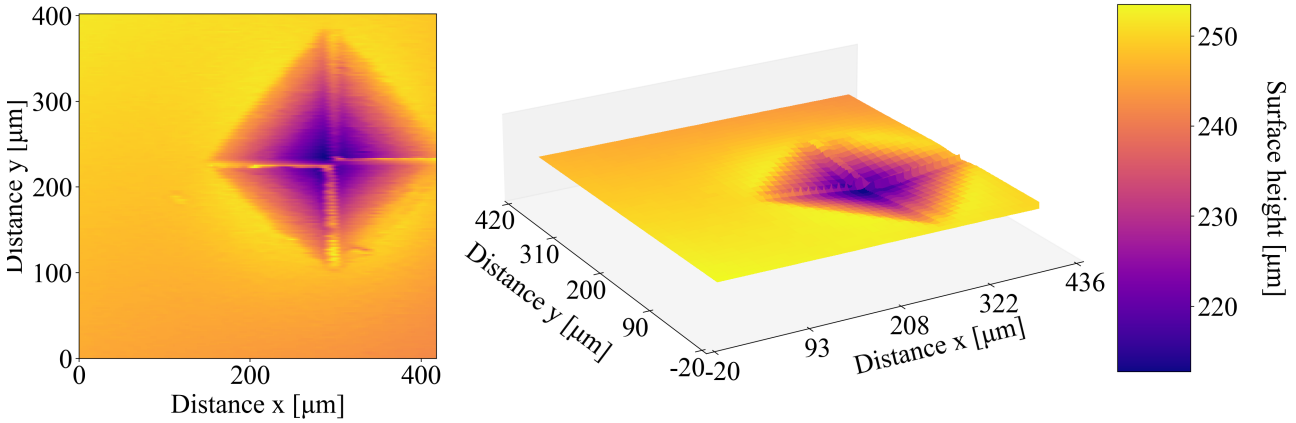


Figure A1: Surface profile data for unirradiated parent Eurofer97 indented with an $H_V10$ Vickers indent.

# Appendix: Characterisation of Laser-welded Eurofer97 Under Proton-irradiation

## A1 Surface Profile Analysis

The proton-irradiation process left the surfaces of the Eurofer97 weld samples stained in the irradiated regions. The staining was examined under energy-dispersive x-ray (EDX) spectroscopy, finding that there had been a fine deposition of indium which contributed to part of the staining. Smaller stain features were prevalent, but too thin to be characterised with EDX, these were likely oxidation effects despite heating occurring in vacuum.

Before attempting to remove the staining a study was performed on unirradiated Eurofer97 to establish the thickness of material that would be removed, out of concern for the thin irradiated layer. A deep $H_V10$ indent was made as a reference depth and then polished using 1/4 µm diamond and 40 nm OPS at 10 minute intervals. Between each step of polishing the surface was examined using a NanoFocus µScan Custom laser-profiler, shown in figure A1. An implicit assumption here is that the apex of the indent was not greatly affected by each polishing step; fine features at the deepest point did not show change over the polishing steps.

The measured surface height was then taken relative to the indent tip and was found not to change up to 30 minutes of polishing with diamond and 30 minutes of polishing with OPS. Given the statistical scatter associated with establishing the tip of the indent, this reading is accurate to within a micron, allaying concern over excessive removal of the irradiated layer.

The laser profilometer was also used to establish surface roughness of the samples. Minimising surface distortion is key to attaining a high quality TGS signal. Scans again established surface height, $z(x)$, from which surface roughness, $R_a$, can be calculated (per BS EN ISO 4287-1998+A1-2009)[? ] as

$$R_a = \frac{1}{l_r}\int_0^{l_r} |z(x) - \bar{z}(x)|dx, \tag{A1}$$

with $\bar{z}(x)$ as the local average profile height and $l_r$ the length of the line over which roughness is calculated. Resultant surface roughnesses for each of the irradiated samples can be found in table A1.

Table A1: Surface roughness parameter for Eurofer97 samples examined in the present work.

| Sample Number | $R_a$ [nm] |
|---|---|
| 1 | 108(6) |
| 2 | 89(6) |
| 3 | 118(15) |
| 4 | 100(7) |

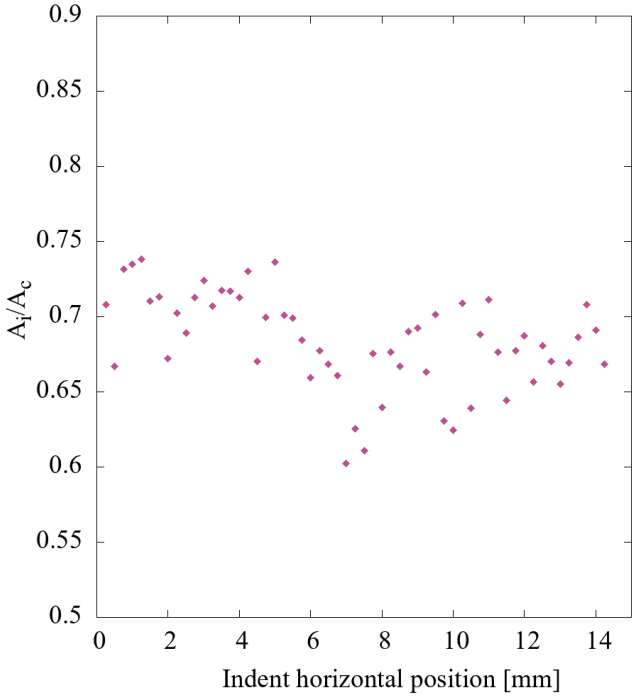


Figure A2: Ratio of nanoindenter inferred projected contact area, $A_i$, to area measured in an SEM image, $A_c$, in the welded Eurofer97 sample taken to 0.31(2) dpa. Indents were taken starting from the parent material, left, toward the weld centre, right.

Errors for surface roughness were primarily statistical, variation between linescans was much larger than the per-point error. Good TGS signals were found with this level of surface roughness.

## A2 Inferred Projected Contact Area

In assessing the accuracy of the projected contact area inferred by the nanoindenter, SEM images were taken of 57 indents across an irradiated sample. These started in the unirradiated parent material, moving across the irradiated parent to the irradiated weld and finally the unirradiated weld. Images were then processed using the ImageJ software package, calibrated using the scale-bar embedded by the SEM software, to find the true projected contact area and assess pile-up. A comparison of the inferred and the true contact area is presented in figure A2, showing there is a significant discrepancy between the two measurements. The correction term for parent and weld material was then formed from these data.

## A3 Nanoindentation Machine Compliance

To evaluate the impact of the nanoindenter apparatus on measurements a varied-load study, using the same experimental equipment as was described in the methods section, a fused silica sample was

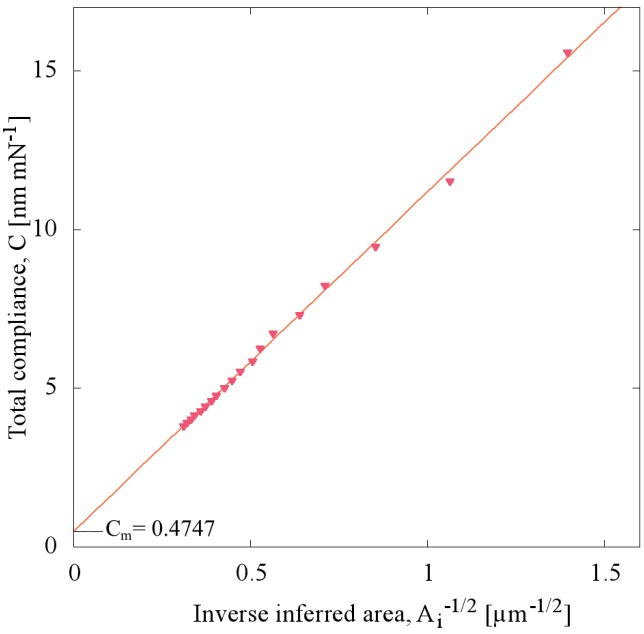


Figure A3: Varied-load data for diamond Berkovich nanoindents in silica.

chosen for its well understood mechanical properties. Total compliance, $C$, is defined as inverse stiffness and can be considered in this case to be acting as two springs in series: one for the sample, $C_s$, and one for the machine, $C_m$:

$$C \equiv \frac{1}{S} = C_m + C_s. \tag{A2}$$

Given that the value sought is the contact area, extracted using stiffness gathered from raw data slope, a correction to this extraction can be made to include only the stiffness of the sample. This starts from the relation of stiffness and contact area[? ]

$$S = 2E_r \sqrt{\frac{A_i}{\pi}}, \tag{A3}$$

where $E_r$ is the reduced Young's modulus defined by the Young's modulus and Poisson ratio of indenter tip, $E_d$ and $\nu_d$, and the sample, $E$ and $\nu$, respectively:

$$\frac{1}{E_r} = \frac{1-\nu^2}{E} + \frac{1-\nu_d^2}{E_d}. \tag{A4}$$

Combining equations A2 & A3 an expression that isolates the machine compliance using readily available data can be obtained

$$C = C_m + \frac{1}{2E_r}\sqrt{\frac{\pi}{A_i}}. \tag{A5}$$

Inverse stiffness is plotted against inverse inferred area in figure A3 for fused silica at loads varying from 1 – 100 mN. Showing a machine compliance value $C_m = 0.4747\,\mathrm{nm\,mN^{-1}}$. This value represents 6.2% of the average compliance in as-welded parent Eurofer97, although this proportion can be as high as 14.2% due to the scatter in these data. The effect of altering compliance on resultant nanohardness was investigated using a dataset taken in parent Eurofer97, varying compliance by up to 30%. Results, shown in figure A4, show that there is a variation of nanohardness with compliance both in average and distribution, with this variation becoming statistically significant at 15% variation from the un-corrected value. This work, therefore, does not include the correction. For less compliant materials (of interest to the field of fusion materials would be tungsten and its alloys, among others)

this factor may be more prominent, for which a first-order correction factor to the inferred contact height may be used

$$h_{c,C_m} = h_{max} - \epsilon P_{max} (C - C_m) . \tag{A6}$$

## A4 Irradiation Current

On-stage current was recorded for each irradiation performed in the current work, the time profile is presented in figure A5. Weld sections were irradiated for around 8 hours each day; the final irradiation day of the heat-treated weld was cut short.

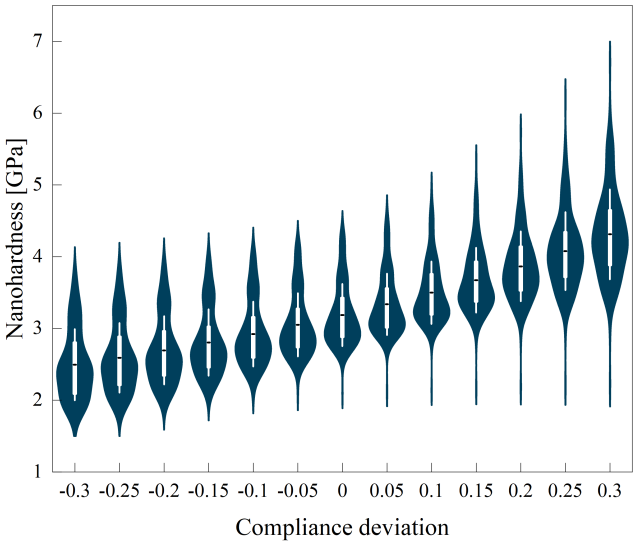


Figure A4: Violin-box-plot displaying the effect of variable compliance on output nanohardness calculation for as-welded parent Eurofer97. White boxes represent the inter-quartile range with a mean black line and single standard deviation whiskers.

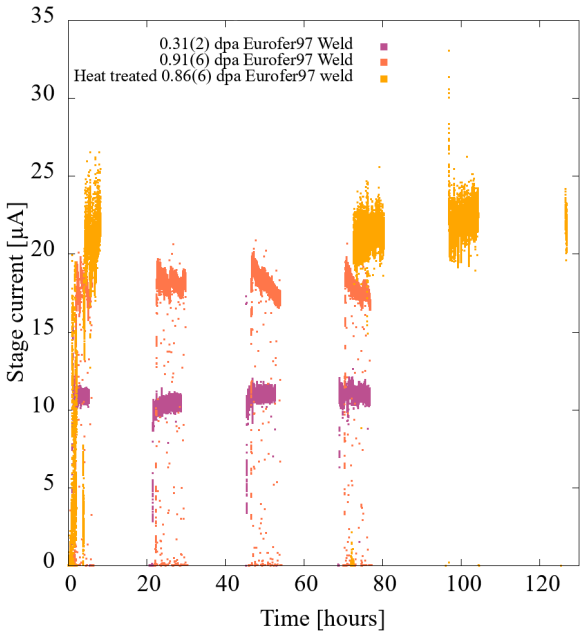


Figure A5: Stage current felt by each sample in this work.

## A5 Irradiation Temperature Correction

The Mansur correction for the different dose rates between protons and neutrons, maintaining a constant defect recombination rate, is of the form:

$$T_2 - T_1 = \frac{\frac{kT_1^2}{E_m^v + 2E_v^f} \ln\left(\frac{G_2}{G_1}\right)}{1 - \frac{kT_1}{E_m^v + 2E_v^f} \ln\left(\frac{G_2}{G_1}\right)}. \tag{A7}$$

$T_1$ is neutron irradiation temperature, $T_2$ proton irradiation temperature, $E_m^v$ is the vacancy migration energy, $E_v^f$ vacancy formation energy, with $G_1$ and $G_2$ as defect production rates from the neutron and proton irradiations, respectively.*†

Applying this concept to the steels irradiations of this work using a neutron irradiation temperature $T_1 = 450\,^{\circ}\mathrm{C}$, a DEMO neutron dose rate $G_1 \propto 3.24{\times}10^{-7}$ dpa $\mathrm{s}^{-1}$ (based on a lifetime dose of 70 dpa over 30,000 2-hour pulses),‡ an expected proton dose rate of $G_2 \propto 5.76{\times}10^{-6}\,\mathrm{dpa\,s^{-1}}$ (dose rate and defect production rate are assumed proportional, and so in this instance are interchangeable), a vacancy formation energy of 1.6 eV and a vacancy migration energy of 0.63 eV§ yields a proton irradiation temperature $T_2 = 486\,^{\circ}\mathrm{C}$.

*L. K. Mansur, *Journal of Nuclear Materials* 206 (1993) 306-323

†G.S.Was, *Fundamentals of Radiation Materials Science*, Springer Science (2007)

‡G. Federici et al., *Fusion Engineering and Design*, (2019), 30-42, 141

§J. Wharry & G. S. Was, *Acta Materialia*, (2014), 42-55, 65